

DOI: 10.1002/adma.200800326

Solution Processed Photovoltaic Devices with 2% Infrared Monochromatic Power Conversion Efficiency: Performance Optimization and Oxide Formation

By *Ethan J. D. Klem, Dean D. MacNeil, Larissa Levina, and Edward H. Sargent**

The necessity of developing economically-sustainable clean energy technologies underpins the search for new materials and device architectures for future generations of solar cells. Solution processed materials offer the promise of flexible and inexpensive production only if they can achieve power conversion efficiencies in excess of 10%. The best solid-state solution-processed solar cells have to date produced power conversion efficiencies in the range 1–5%.^[1,2] One factor limiting their further improvement is their lack of infrared energy capture. Half of the sun's power reaching the earth lies beyond 700 nm, and one third beyond 1000 nm. Many of the promising material systems today that have started to reach into the infrared spectrum still have their absorption peaks lying near to the visible spectral regime. This includes high performing inorganic thin-film nanocrystal-based devices with an absorption edge at about 700 nm, and organic polymer-fullerene derivatized devices effective out to about 1000 nm (with a peak efficiency lying at 800 nm).^[1,3] An effective means of increasing overall solar cell efficiency using new thin-film materials can be had through the use of tandem or multi-junction solar cells.^[4] Although the optimum band-gap for a single junction device lies at about 1100 nm, the optimum band-gaps for a two junction cell are 760 nm and 1320 nm, and for a three junction cell are 1750 nm, 1070 nm, and 680 nm.^[5] As the number of junctions increases in a solar cell so does the maximum power conversion efficiency, increasing from 32.5% to 49.7% (under unconcentrated illumination) as one progresses from a single junction to a triple junction cell.

For these reasons, the use of short-wavelength infrared-sensitive quantum dots with an absorption edge tunable from 900 to 1800 nm have been pursued to access the portion of the solar spectrum not currently absorbed by most other solution processed materials.^[6–8] In 2007 we reported on a PbS nanocrystal-based photovoltaic device with record monochromatic infrared power conversion efficiencies of 1.3%. In these devices we employed ethanedithiol as a bidentate-crosslinking ligand during the deposition of our colloidal quantum dot (CQD) film onto a rough, porous ITO matrix. We observed

that device performance could be improved markedly through air annealing and by doing so increased the power conversion efficiency by two orders of magnitude, resulting in the record performance reported.^[6]

Annealing has also been successfully used to improve the performance in other nanocrystal-base devices.^[11,6,9] A recent report on binary nanoparticle superlattices found that the maximum p-type conductivity came about after heating in air ambient to 150 °C.^[9] Similarly, a report on CdSe/CdTe nanorod heterojunction devices noted that long exposure to air increased the open circuit voltage.^[11]

In bulk and microcrystalline semiconductor devices annealing and oxide growth have been shown to be useful in influencing device performance by altering the energy distribution and density of interface-induced mid-gap states. For devices based on semiconductor heterojunctions, such as microcrystalline CdS/CdTe solar cells, control of the interface states is a primary determinant in device power conversion efficiencies.^[10] In Schottky-junction devices the interface induced gap states are the fundamental mechanism that determines the barrier heights of the Schottky contact.^[11] Furthermore, in bulk and microcrystalline Schottky junction photovoltaic devices altering the composition and extent of the interface layer between the metal and the semiconductor is seen as a key factor influencing the open circuit voltage of the solar cell.^[12–14]

To improve on the photovoltaic performance previously reported we set out to systematically optimize our devices and gain insight into the material changes that contribute to the performance improvements. As annealing is clearly playing an important role we sought to understand if the benefits were gained from the heating alone (for example through removal of insulating ligands and associated increase in charge transport properties) or if changes in the nature and extent of the oxidation products produced during air annealing were contributing to the performance benefits observed. As a result of these efforts we herein report an infrared power conversion efficiency of 2%, representing a new record in the infrared power conversion efficiency of solution-processed SWIR photovoltaics.

We first fabricated a series of devices which consisted of a porous ITO electrode infiltrated with butylamine ligand-exchanged, solution-synthesized PbS nanocrystals. These devices are then capped by a Mg contact.^[6] Our ligand exchange procedure results in substantial replacement of the original strongly-bound oleic acid ligand (carboxylate end functional group)

[*] Prof. E. H. Sargent, E. J. D. Klem, Dr. D. D. MacNeil, Dr. L. Levina
Department of Electrical and Computer Engineering, University of Toronto
Toronto, Ontario, M5S 3G4, Canada
E-mail: ted.sargent@utoronto.ca

with butylamine ligand (amine end functional group). This procedure reduces the interparticle spacing, improving electrical conductivity in the CQD films but also replaces the oleic acid with the more labile, and more volatile butylamine.^[15]

The device fabrication consists of dip coating the ITO electrode into a 4% by volume solution of ethanedithiol in acetonitrile and then dipping the substrate into a dilute solution of PbS nanocrystals. This process was then repeated three times. In this device architecture infrared light is absorbed in the PbS nanocrystals and the electrons associated with this excitation escape into the top Mg contact at a metal-semiconductor Schottky junction while the holes travel into the ITO electrode. A schematic of this device is shown in the inset of Figure 2a. The polarity of the short-circuit currents observed when the devices are operated under illumination is consistent with the picture of the extraction of electrons into the metal and holes into the ITO (that is, the short circuit current is positive when the ITO is held at zero volts).

Once fabricated, a set of devices were annealed in air at 110 °C, 130 °C, and 150 °C for three hours. Another set of devices were annealed under inert conditions in a vacuum oven at 110 °C, 130 °C, and 150 °C for three hours. An additional device was also set aside without annealing. These devices all then had their top metal contact deposited by thermal evaporation.

The absorption spectrum of PbS nanocrystals was examined before ethanedithiol treatment, after ethanedithiol treatment, and after three hours of heating at 130 °C. All three samples showed a clear exciton absorption peak indicating that quantum confinement remained and that the nanocrystals had not been sintered into an amorphous or microcrystalline thin film.

As-fabricated, without annealing, the devices exhibited a very weak photovoltaic effect with open circuit voltages of less than 100 mV under 970 nm monochromatic infrared illumination and external quantum efficiencies (EQEs) of 0.2%.

The vacuum annealed devices showed a trend of increasing EQE with increasing temperature (Fig. 1b). Here EQE improved from 1% after 110 °C inert annealing up to 6% after 150 °C. However, the open-circuit voltage remained low (Fig. 1a) at ~90 mV for all inert annealing temperatures tested. Figure 1c shows the maximum power conversion efficiency under monochromatic illumination is 0.08%. We provide the *J-V* characteristic under monochromatic illumination in Figure 2a of the device heated in vacuum at 150 °C.

The device annealed under air showed more pronounced photovoltaic performance gains with external quantum efficiency, open circuit voltage and power conversion efficiency all increasing with increased temperature. The EQE of these devices (Fig. 1b) increased to 8% after annealing at 110 °C and to 18% after 150 °C annealing. The open circuit voltage under monochromatic IR illumination showed a marked increase from an initial 100 mV without annealing to 425 mV after 150 °C air annealing. Figure 1a shows the trend of larger open circuit voltages with higher processing temperatures. Finally, the power conversion efficiency (Fig. 1c) increased to 2% at the 150 °C annealing temperature. The 2% power conversion

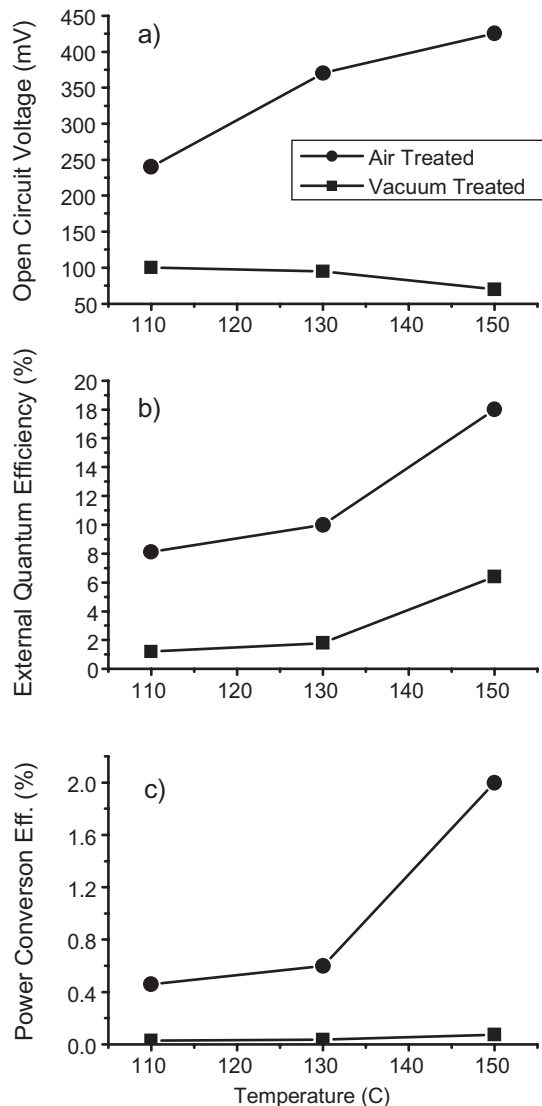


Figure 1. Photovoltaic device performance characteristics for devices treated in air and vacuum at different temperatures. All measurements were taken under monochromatic 975 nm illumination at 12 mW cm⁻². a) Shows that an increase in open circuit voltage only occurs when the PbS CQD solid is annealed in air. b) Indicates the increase in external quantum efficiency attributed to improved charge transport characteristics after heating. Air annealing devices has a marked impact on power conversion efficiency as indicated in (c), with a maximum infrared power conversion efficiency shown of 2%.

efficiency achieved here represents a 54% improvement over that reported in earlier work.^[6] We provide the *J-V* characteristic under monochromatic illumination in Figure 2b of the device annealed at 150 °C.

To examine the stability of our best performing devices we stored them in air for 6 months, after which we characterized them again. The Mg contacts themselves had oxidized, so we deposited new contacts on the air-treated colloidal quantum dot films. Aged devices retained the bulk of their performance, diminishing approximately 20% in power conversion efficiency compared to fresh devices. We also studied the effect of

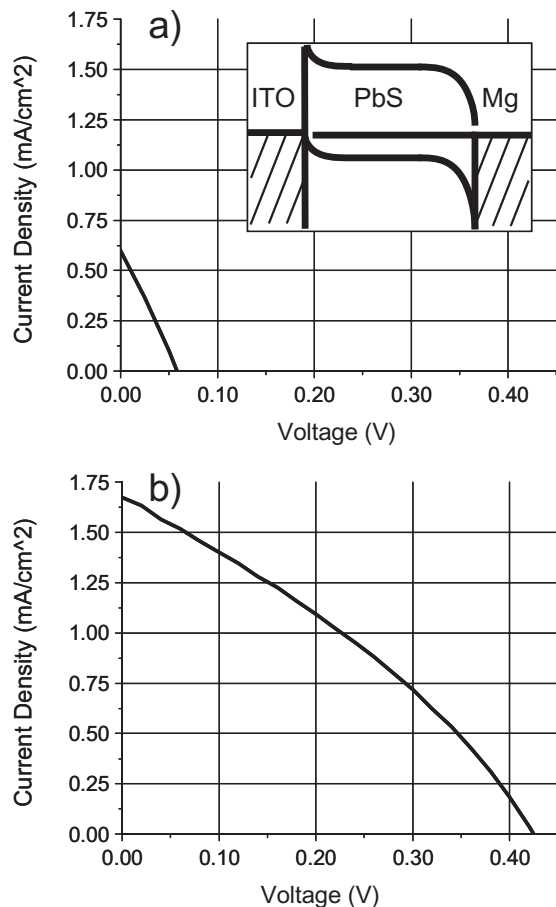


Figure 2. Shows the photovoltaic performance of two different devices, one heated in vacuum at 150 °C (a) and one heated in air at 150 °C (b) under monochromatic 975 nm illumination at 12 mW cm⁻². The inset of (a) shows a schematic of the junctions formed between the PbS CQD solid and the Mg and ITO contacts.

heating the devices in air at 90 °C to examine the stability under accelerated ageing conditions. Devices heated in this manner for 14 hours showed no appreciable change in performance. A more thorough aging study of these devices is required to expand this initial picture of air stability.

A number of trends were observed during our device optimization study. First, heating in inert or air atmospheres led to an increase in EQE. Second, annealing alone was not sufficient to increase open circuit voltage; annealing in air was required to produce the observed 300% increase in open circuit voltage. We hypothesize that air annealing results in a partial oxidation of our films that is otherwise absent when our nanocrystals are annealed in inert atmospheres. But what is the nature of this oxidation? Are there certain oxidation products that are formed to a greater or lesser extent with differing impacts on device performance? What changes are occurring as a result of heating alone? We hypothesize that ligand loss is occurring during heating, but what species of ligands are being removed and at what temperatures? To investigate and explore these questions we used thermogravimetric analysis (TGA),

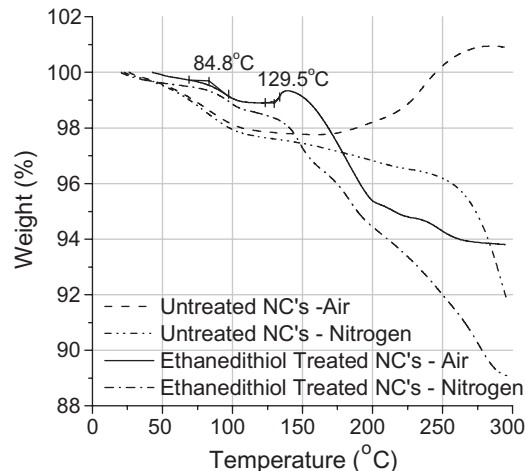


Figure 3. TGA of a PbS nanocrystals in air and nitrogen before ethanedithiol (EDT) treatment. TGA is also shown for PbS after treatment with ethanedithiol and was done in air and in nitrogen. Evidence of oxidation is shown by the weight increase that occurs for both the air heated samples. The ethanedithiol treated samples were rinsed in acetonitrile before TGA was performed in order to reduce the content of thiols that are not coordinated to the nanocrystal surface. The onset point seen at about 85 °C in the ethanedithiol treated samples in both air and nitrogen likely corresponds to the decomposition of butyl amine as butyl amine has a boiling point of 78 °C.

head-space gas-chromatography mass-spectroscopy (HS-GCMS), Fourier transform infrared spectroscopy (FTIR), and X-ray photoelectron spectroscopy (XPS) to provide information about our materials at each of their processing stages.

We present the summary of the results of these studies in Table 1. Here we show that untreated PbS nanocrystals initially contain PbSO₄, PbSO₃, and PbO. After treatment with ethanedithiol the PbO content is greatly reduced (and is in fact, undetectable in our measurements) while the PbSO₄ and PbSO₃ content increases. Not surprisingly, nanocrystals heated in inert atmospheres show no change in the extent of oxidation. However, the samples heated in air show a return of PbO, a small increase in PbSO₄ and a larger increase in PbSO₃.

To discuss the details of our experiments we first examine the TGA of butyl-amine exchanged PbS nanocrystals. TGA measurements were carried out in both air and in nitrogen on nanocrystal CQD solids drop cast from solution. Samples were tested with ethanedithiol treatment and without ethanedithiol treatment with the results shown in Figure 3. We observed an increase in mass above ~100 °C in both the ethanedithiol

Table 1. Summary of material changes observed in PbS nanocrystals during device treatment and fabrication procedure.

	PbO	PbSO ₄	PbSO ₃
Untreated Nanocrystals	present	present	present
Ethanedithiol Treated NCs	absent	↑	↑
Air Annealed Nanocrystals	↑	small ↑	↑
Inert Annealed Nanocrystals	no change	no change	no change

treated and untreated samples when air heated but not when heated in nitrogen. The ethanedithiol treated samples show a further increase in mass between 130 °C and 150 °C, a temperature range corresponding to that used to obtain optimal device performance. We attribute the observed increase in sample mass to oxidation. We also observe a reduction in mass starting at ~85 °C which we attribute to the decomposition of butyl amine as butyl amine has a boiling point of 78 °C. To confirm this hypothesis we turn to HS-GCMS.

HS-GCMS was employed on ethanedithiol treated and untreated PbS nanocrystals. As the samples were heated amine species were detected at both the 80 °C range and the 125 °C range, confirming that there are butyl-amine ligands being removed from the PbS during heating. In the ethanedithiol treated samples, sulphur species were not detected until the 200 °C temperature range, indicating that the thiol-nanocrystal coordination is much stronger than between PbS and the amine-terminated ligands. To summarize: TGA and HS-GCMS have shown that oxidation is occurring in the CQD films during annealing in air and that butyl-amine ligands are being removed during annealing in both air and inert atmospheres.

To further explore the nature of the compositional changes that occur in PbS CQD solids during device fabrication we turn to Fourier transform infrared spectroscopy (FTIR). Butylamine ligand-exchanged PbS nanocrystal films were drop-cast from solution onto infrared (IR)-transparent windows and allowed to dry in nitrogen. We first examine nanocrystals that had been stored in solution in inert (nitrogen glovebox) and ambient atmospheres. The FTIR spectra reveals the presence of PbO and PbSO₄ in our as-drop cast films. Figure 4a shows the spectra of an untreated PbS sample stored in an inert atmosphere and a PbS sample store under ambient conditions. These spectra are accompanied by a reference spectrum of PbO powder. We focus our attention on the peak at 3437 cm⁻¹ which serves as a fingerprint for PbO and peaks at 1161 cm⁻¹ and 1033 cm⁻¹ which serve to identify PbSO₄.^[16]

Figure 3a reveals that PbO and PbSO₄ are readily formed on nanoparticles under certain storage conditions. Only the strictest inert atmosphere and dry solvent processing led to nanocrystal films possessing no identifiable PbO or PbSO₄ content. Nanocrystals stored under ambient conditions readily oxidize.

As water has a strong absorption peak centered at about 3392 cm⁻¹ we also carried out a set of experiments tracking our PbO fingerprint feature in the presence of water which served to confirm that this feature is independent of water content (Fig. S1).

We then examine the FTIR spectra of nanocrystal films treated with ethanedithiol (Fig. 4b) as compared to that without ethanedithiol treatment. The most pronounced result of this comparison is that the PbO feature is almost entirely absent after ethanedithiol treatment. In contrast to this observation the PbSO₄ feature is present before and after thiol treatment. PbS films were also treated with different-length thiol-terminated ligands, including butanethiol and hexane-dithiol, both of which were shown to be effective in the removal of PbO in nanocrystal films. The composition at of the

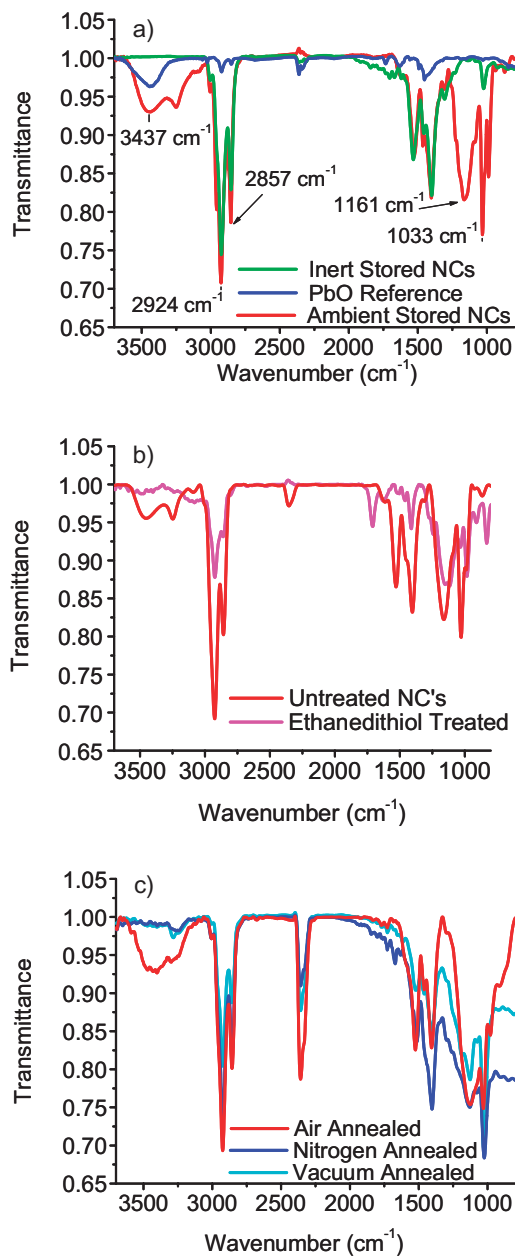


Figure 4. a) FTIR spectra of untreated PbS nanocrystals, PbO reference spectrum and a PbS nanocrystal sample stored under ambient conditions for three days. The peak labeled at 3437 cm⁻¹ is used to identify the presence of PbO. The peaks labeled at 1161 cm⁻¹ and 1033 cm⁻¹ are associated with PbSO₄. The peaks labeled at 2924 and 2857 cm⁻¹ are associated with C–H bonds present in the butylamine ligands and in the remaining oleic acid ligands. In thiol treated samples where these ligands are expected to be predominately displaced by thiol functionalized ligands, these features correspond to the C–H stretches in the new thiol ligands. While the inert stored PbS does not show any observable spectral feature at 3437 cm⁻¹, after ambient storage the PbS film shows the emergence of the PbO spectral feature. b) FTIR spectra of untreated PbS films and films rinsed with solutions of 4% ethanedithiol in acetonitrile for 10 minutes. The lack of a discernable PbO feature indicates that the thiols have reduced the PbO content. c) FTIR spectra of PbS nanocrystals rinsed with 4% ethanedithiol in acetonitrile for 10 minutes followed by heating at 130 °C for 2 hours in vacuum, nitrogen and air. The PbO peak at 3437 cm⁻¹ is re-introduced only in the sample heated in air.

CQD films at this stage of processing is of interest because it corresponds to the photovoltaic devices immediately after fabrication, before devices have been subject to any annealing.

To confirm our FTIR findings regarding PbO reduction vis-à-vis thiol treatment X-ray photoelectron spectroscopy (XPS) was utilized to examine the oxidation state of the elements present in our materials. The O1s spectra was obtained for nanocrystals stored under ambient conditions (Fig. 5a), which were then treated with ethanedithiol (Fig. 5c). Deconvolution of the spectrum confirms the presence of PbO in the untreated nanocrystals. After ethanedithiol treatment the O1s spectra shows that the PbO content is substantially diminished, confirming the FTIR findings. Other species identified in the O1s spectra both before and after ethane-

dithiol treatment were PbSO₃, PbSO₄, and SiO₂ (from the Si substrate). The S2p spectrum of the untreated nanocrystals (Fig. 5b) confirms the presence of sulphites and sulphates in our PbS sample. Once treated with ethanedithiol (Fig. 5d) the S2p spectrum shows that in addition to PbSO₃ and PbSO₄, the samples also show the presence of metal-bound thiols as well as unbound thiols.^[17]

The growth of the PbSO₄ peak in the S2p spectra after ethanedithiol treatment (Fig. 5d) relative to the PbS peak suggests a mechanism whereby ethanedithiol reduces the PbO content of PbS nanocrystals by promoting the growth PbSO₄.

Annealing the nanocrystals after ethanedithiol treatment in both ambient and inert atmospheres is the final stage in the device fabrication process before deposition of the top metal

contact. To examine the impact of annealing on the composition of our PbS films we first look at the FTIR spectra of nanocrystals heated in air, nitrogen and vacuum (Fig. 4c). As expected the PbO peak returns after air heating but does not show any growth after nitrogen or vacuum heating. The sulphate feature remains strong in our air annealed sample and does not show any significant change in our inert annealed samples. This is of interest because the air annealing conditions correspond to those required to achieve the largest performance gains in our photovoltaic devices. The inert annealing corresponds to the conditions in the devices heated in vacuum that did not exhibit the same performance gains.

We use XPS to confirm and expand our understanding of the oxidation changes occurring in the air annealed thiol-treated samples. We see in the O1s spectrum (Fig. 5e) that the PbO content has indeed been re-introduced, confirming our FTIR findings. The S2p spectrum of air-heated samples shows that PbSO₃ content has also increased. The PbSO₄ content also remains present in the S2p spectrum after air heating but the deconvolution of the S2p spectrum before and after annealing indicates that the amount of PbSO₄ present relative to PbS has increased only slightly. Air annealing has in effect promoted the growth of PbO and PbSO₃, but not PbSO₄. As a further control we annealed PbS nanocrystals in nitrogen and as expected XPS showed no change in the content of any of our identified oxidation products.

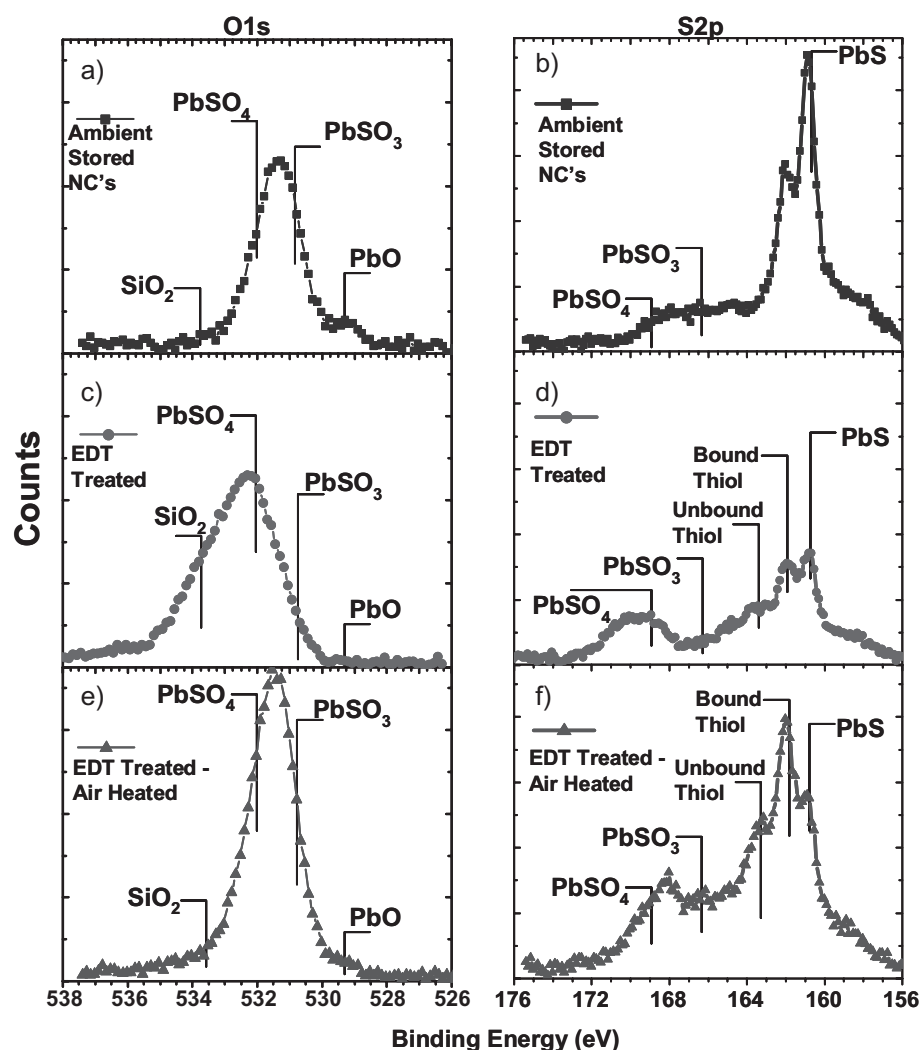


Figure 5. O1s (a,c,e) and S2p (b,d,f) high resolution XPS spectra with peak positions indicated of species identified through spectral deconvolution (details shown in SOM 2-7). a) and b) Untreated PbS nanocrystals. c) and d) Ethanedithiol treated nanocrystals and (e) and (f), ethanedithiol treated nanocrystals which were then by heated in air at 130 °C. The main PbS oxidation products observed are PbO, PbSO₃, and PbSO₄. Although lead sulphite and sulphate are present through all processing conditions the lead oxide content is greatly reduced (or removed) by the thiol treatment. The SiO₂ observed in the O1s spectra is due to the silicon substrate.

The results of the FTIR and XPS measurements show that PbS CQD films after ethanedithiol treatment exhibit a reduction in the PbO content but not the PbSO₃ or PbSO₄ content. Furthermore, air annealing is required to re-introduce PbO content and while doing so simultaneously increases the content of PbSO₃ in the film. Nanocrystals that have been ethanedithiol treated and subsequently annealed in an inert atmosphere retain only their initial PbSO₄ and PbSO₃ content but have no observed PbO content. When these results are viewed alongside the performance of similarly processed photovoltaic devices it appears that the formation of PbO and PbSO₃ is an integral step in obtaining increased open circuit voltages and power conversion efficiencies.

Recent results utilizing semiconductor nanocrystals in electrical devices have shown that many of the properties of bulk semiconductors also apply to solution processed semiconductor nanocrystals. (For example Schottky junctions are formed when conductive PbS CQD films are brought into contact with Al and when ZnO tetrapods are coated with Pt.^[18,19]) In a manner analogous to that seen in bulk metal-semiconductor Schottky photovoltaic cells it is likely that the growth of oxidation products in PbS nanocrystal CQD films leads to the improvements in photovoltaic devices by modifying the mid-gap states formed at nanocrystal boundaries.

In particular the observation that the presence of PbSO₄ (and PbSO₃ in smaller quantities) alone does not significantly impact the open circuit voltage (as is the case in the inert atmosphere annealed devices), indicating that the passivation of mid-gap states is primarily influenced by the formation of PbO and PbSO₃. Using the combination of a thiol-terminated bidentate linker and oxide formation during the fabrication of a photovoltaic device leads to an increase in open circuit voltage from less than 100 mV to 425 mV; and ultimately results in a record 2% infrared power-conversion efficiency in solution-processed photovoltaics.

Experimental

PbS nanocrystal synthesis followed the procedure described previously [20]. The as-prepared nanocrystals were passivated by oleic acid ligands and were exchanged for n-butyl amine ligands following the procedure described by Konstantatos et al. [15]. The exchanged nanocrystals were dispersed in octane.

FTIR analysis was performed by drop-casting nanocrystals from octane onto double-sided-polished undoped silicon substrates. Samples that were treated with thiols (as seen in Fig. 1C) were soaked in a 4% thiol solution in acetonitrile for about 10 minutes. A Bruker Tensor 27 was used for all measurements.

Device fabrication began with the creation of a porous high-surface area electrode. The slurry of Indium Tin Oxide (ITO) employed consisted of 4 g of ITO (Nanotek, Alfa Aesar) and 4 g of distilled water. To this suspension, 2 ml of Triton-X surfactant (Aldrich) was added drop-wise and stirred overnight, 100 μ L of the slurry was then spin-coated (800 rpm, 60 s) onto a 1" square planar ITO coated glass slide. The sample was annealed at 310 °C for 1 hour. The device was then dip-coated with butyl-amine capped nanocrystals in octane with a

concentration of 150 mg ml⁻¹. It was then placed into an acetonitrile solution containing ethanedithiol (Aldrich) at a concentration of 4% by volume. This procedure was repeated three times and resulted in a PbS-infiltrated porous oxide film, as confirmed by cross-sectional SEM and EDX. Devices were then either annealed in either vacuum, or in air, as described in the main text. When the device was ready for testing, the top metal contact was deposited by vacuum evaporation of a 300 μ m-diameter circular pad that consisted of 100 nm of Mg followed by 100 nm of Ag.

Samples for XPS analysis were prepared by drop-casting nanocrystals from octane onto double-sided-polished undoped silicon substrates. Samples that were treated with ethanedithiol were soaked in a 4% thiol solution in acetonitrile for about 10 minutes. The heated sample was heated at 130 °C for three hours in air. The samples were measured at using a PHI 5500 (XPS) Spectrometer.

Analysis of XPS Measurements: Before analysis the binding energy of all XPS spectra were referenced to the C1s hydrocarbon line at 285.0 eV. High resolution O1s spectra were used for examining the evolution of the PbO, PbSO₃, and PbSO₄ content in drop cast nanocrystal films. The S2p high resolution spectra were used for further confirmation of the PbSO₃ and PbSO₄ content.

The deconvolution of the O1s spectra was performed by fitting a sum of Gaussian-Lorentzian functions (always with greater than 80% Gaussian weighting) to the experimental data. PbO was identified using a peak centered at 529.3 eV [21, 22], PbSO₃ was identified using a peak centered at 530.8 eV [23], while PbSO₄ was centered at 531.8 eV [21] and SiO₂ (from the Si substrate) was centered at 533.3 eV.

The deconvolution of the S2p spectra was performed by fitting a sum of Gaussian-Lorentzian functions (always with greater than 80% Gaussian weighting) to the experimental data. Each species was fit with a S2p doublet (due to the presence of S2p_{3/2} and S2p_{1/2} peaks) with a 2:1 area ratio and a splitting of 1.2 eV. PbSO₃ was identified using a S2p_{3/2} peak position of 166–166.6 eV [22, 24]. The PbSO₄ was identified using a peak position of 168–169 eV [22, 24] and PbS identified using a peak position of 160.7–160.8 eV [24, 25]. After treatment with ethanedithiol the samples also show the presence of metal-bound thiols which were identified using a S2p_{3/2} peak position of 161.9 eV [17] and unbound thiols at a peak position 163.5 eV [17].

Samples for TGA were prepared by drop-casting approximately 100 μ l of 150 mg ml⁻¹ solution of butyl-amine exchange PbS nanocrystals in octane onto a glass slide. The films were then soaked in a 4% by volume solution of ethanedithiol in acetonitrile for approximately 5 minutes followed by an acetonitrile rinse to remove un-bound thiols. The samples were then scraped off into sample holders for the TGA experiment.

Received: February 1, 2008

Revised: April 18, 2008

Published online: July 15, 2008

- [1] I. Gur, N. A. Fromer, M. L. Geier, A. P. Alivisatos, *Science* **2005**, *310*, 462.
- [2] W. L. Ma, C. Y. Yang, X. Gong, K. Lee, A. J. Heeger, *Adv. Funct. Mater.* **2005**, *15*, 1617.
- [3] X. J. Wang, E. Perzon, F. Oswald, F. Langa, S. Admassie, M. R. Andersson, O. Inganäs, *Adv. Funct. Mater.* **2005**, *15*, 1665.
- [4] J. Y. Kim, K. Lee, N. E. Coates, D. Moses, T. Q. Nguyen, M. Dante, A. J. Heeger, *Science* **2007**, *317*, 222.
- [5] A. Marti, G. L. Araujo, *Sol. Energy Mater. Sol. Cells* **1996**, *43*, 203.
- [6] E. J. D. Klem, D. D. MacNeil, P. W. Cyr, L. Levina, E. H. Sargent, *Appl. Phys. Lett.* **2007**, *90*.
- [7] A. Maria, P. W. Cyr, E. J. D. Klem, L. Levina, E. H. Sargent, *Appl. Phys. Lett.* **2005**, *87*.

- [8] S. A. McDonald, G. Konstantatos, S. G. Zhang, P. W. Cyr, E. J. D. Klem, L. Levina, E. H. Sargent, *Nat. Mater.* **2005**, *4*, 138.
- [9] J. J. Urban, D. V. Talapin, E. V. Shevchenko, C. R. Kagan, C. B. Murray, *Nat. Mater.* **2007**, *6*, 115.
- [10] J. Fritsche, A. Klein, W. Jaegermann, *Adv. Eng. Mater.* **2005**, *7*, 914.
- [11] *Wide-Gap Chalcopyrites*, (Eds: S. Siebantritt, V. Rau), Springer, Heidelberg, Germany **2006**.
- [12] S. R. B. Lepley, *Phys. Status Solidi A* **1976**, *33*, 517.
- [13] M. Peckerar, M. Peckerar, H. C. Lin, R. L. Kocher, presented at the Int. Electron Devices Meeting, Washington D.C., December 1975.
- [14] H. Tsubomura, H. Kobayashi, *Crit. Rev. Solid State Mater. Sci.* **1993**, *18*, 261.
- [15] G. Konstantatos, I. Howard, A. Fischer, S. Hoogland, J. Clifford, E. Klem, L. Levina, E. H. Sargent, *Nature* **2006**, *442*, 180.
- [16] G. L. J. Trettenhahn, G. E. Nauer, A. Neckel, *Vibrational Spectrosc.* **1993**, *5*, 85.
- [17] D. G. Castner, K. Hinds, D. W. Grainger, *Langmuir* **1996**, *12*, 5083.
- [18] J. P. Clifford, K. W. Johnston, L. Levina, E. H. Sargent, *Appl. Phys. Lett.* **2007**, *91*, 253117.
- [19] M. C. Newton, S. Firth, P. A. Warburton, *Appl. Phys. Lett.* **2006**, *89*.
- [20] M. A. Hines, G. D. Scholes, *Adv. Mater.* **2003**, *15*, 1844.
- [21] P. Nowak, K. Laajalehto, I. Kartio, *Colloids Surf. A* **2000**, *161*, 447.
- [22] L. Cademartiri, G. von Freymann, A. C. Arsenault, J. Bertolotti, D. S. Wiersma, V. Kitaev, G. A. Ozin, *Small* **2005**, *1*, 1184.
- [23] D. S. Zingg, D. M. Hercules, *J. Phys. Chem.* **1978**, *82*, **1992**.
- [24] S. R. Grano, C. A. Prestidge, J. Ralston, *Int. J. Mineral Proc.* **1997**, *52*, 1.
- [25] R. B. Shalvoy, G. B. Fisher, P. J. Stiles, *Phys. Rev. B* **1977**, *15*, 1680.